



UNIVERSITY OF LEEDS

This is a repository copy of *A liquid marble method for synthesizing large-sized carbon microspheres with controlled interior structures*.

White Rose Research Online URL for this paper:
<https://eprints.whiterose.ac.uk/176034/>

Version: Accepted Version

Article:

Xue, N, Cao, J, Zhang, X et al. (4 more authors) (2021) A liquid marble method for synthesizing large-sized carbon microspheres with controlled interior structures. *Carbon*, 179. pp. 541-553. ISSN 0008-6223

<https://doi.org/10.1016/j.carbon.2021.04.060>

© 2021, Elsevier. This manuscript version is made available under the CC-BY-NC-ND 4.0 license <http://creativecommons.org/licenses/by-nc-nd/4.0/>.

Reuse

This article is distributed under the terms of the Creative Commons Attribution-NonCommercial-NoDerivs (CC BY-NC-ND) licence. This licence only allows you to download this work and share it with others as long as you credit the authors, but you can't change the article in any way or use it commercially. More information and the full terms of the licence here: <https://creativecommons.org/licenses/>

Takedown

If you consider content in White Rose Research Online to be in breach of UK law, please notify us by emailing eprints@whiterose.ac.uk including the URL of the record and the reason for the withdrawal request.



eprints@whiterose.ac.uk
<https://eprints.whiterose.ac.uk/>

A liquid marble method for synthesizing large-sized carbon microspheres with controlled interior structures

Nan Xue ^{a,1}, Jie Cao ^{a,1}, Xiaoming Zhang ^a, Congming Li ^b, Rammile Ettelaie ^c, Xian Liu ^a, and Hengquan Yang ^{a,*}

[a] School of Chemistry and Chemical Engineering, Shanxi University, Taiyuan 030006, China

[b] Key Laboratory of Coal Science and Technology, Ministry of Education and Shanxi Province, Taiyuan University of Technology, Taiyuan 030024, China.

[c] Food Colloids Group, School of Food Science and Nutrition, University of Leeds, Leeds LS2 9JT, United Kingdom.

¹ These authors contributed equally to this work.

*To whom correspondence should be addressed: hqyang@sxu.edu.cn (Hengquan Yang)

Abstract

Millimeter-sized porous carbon spheres (MPCS) with both controllable interior architecture and high mechanical strength are highly desired for practical applications, but there is no efficient method to synthesize these materials. Here, we report a strategy to fabricate millimeter-sized porous carbon spheres by harnessing the liquid marble phenomenon. This strategy enables us to obtain a series of MPCS with tunable interior architectures, such as honeycombed MPCS, foam-like MPCS, cavity-containing MPCS and hollow MPCS, which add new members to carbon microsphere family. Crucially, the mechanical strength of MPCS reaches as high as 14.6 N, favoring its practical applications. Moreover, our protocol allows for nitrogen element and metal to be in situ incorporated within the body of MPCS, leading to an efficient catalyst for levulinic acid (LA) hydrogenation or benzene hydrogenation. Impressively, turnover numbers (TONs) of 113000 in the LA hydrogenation and 480 h of continuous benzene hydrogenation with TONs of 116000 are achieved, which highlights the potential in engineering applications of these novel microspheres.

1. Introduction

Driven by ever-increasing applications in catalysis, gas sorption, water treatment and energy storage, synthesis of carbon microspheres with porous architecture, controllable size, and high mechanical strength, has become an important scientific and technological goal [1-10]. The past three decades have witnessed the successful fabrication of various carbon microspheres, including yolk-shell [11-12], core-shell [13-14] and hollow architectures [15-17]. However, these achievements are largely limited to carbon materials whose sizes range from nanometers to a few microns. From the practical points of view, spherical particles as large as millimeter are also highly desirable at least because the large particle size is very crucial for continuous process, separation and recycling [18-19]. For example, millimeter-sized carbon spheres can be directly packed in industrially preferred fixed-bed reactors for continuous catalysis, thus overcoming the notorious problems associated with addition of binders to form larger shaped objects from the smaller-sized carbon materials [20-22].

However, fabrication of large-sized carbon spheres with tunable interior architecture and high mechanical strength is extremely challenging. This is because it is very difficult to delicately control their interior structure and maintain uniformity on a micron-to-millimeter scale. Emulsification [23-24], microfluidics [25-26] and spray drying [27] methods have all been exploited to synthesize micron-level carbon materials. For instances, Long and co-workers used an emulsification method to prepare porous carbon spheres with sizes in the range of tens to hundreds of microns [28]. Very recently, our group successfully developed a Pickering emulsion based method to fabricate micron carbon spheres [29]. Shi et al. utilized surfactant-based emulsions to synthesize approximately 1 mm carbon spheres, but the resulting carbon spheres lacked the required hierarchical pore structure within their body [30]. Liu et al. employed microfluidic devices to manufacture carbon spheres with diameters of several hundreds of microns [31]. The spray drying method was only suitable to generate carbon spheres of nano-to-micron size [32-33]. Despite the significant progress in synthesis of carbon microspheres, the existing methods are still unable to access carbon spheres in millimeter-sized range, having tunable interior pore structures while also exhibiting high mechanical robustness. The main reasons for this arise from two sources: (i) The droplets needed in these methods tend to be deformable when their

dimensions are large and comparable to millimeter length scales. This prevents such methods from achieving a uniform morphology; (ii) It is not trivial to control the kinetics of the polymerization across nanometer to millimeter scale, thereby being unable to control the interior structure. In this context, development of an effective strategy for fabrication of porosity-tunable, millimeter-sized, mechanically robust carbon spheres remains a challenging task.

Herein, we report, for the first time, a liquid marble method to fabricate millimeter-sized porous carbon spheres (MPCS) possessing high mechanical strength. We demonstrate how to tune the interior structure of the particle, their size, their N-functionalization and their mechanical strength. Hitherto unreported, honeycombed, foam-like, cavity-containing and hollow MPCS integrating micro, meso and macro pores were obtained. The fundamental principles underpinning the formation of MPCS and the insights into the structural evaluation are discussed. Furthermore, our method is demonstrated to allow Ru nanoparticles to be in situ embedded into the body of MPCS, leading to efficient catalysts towards levulinic acid (LA) hydrogenation and benzene hydrogenation. We envisage this work opens a new methodology for fabrication of large-sized carbon microspheres and relevant catalysts for a range of useful practical applications.

2. Experimental section

2.1. Chemicals

Resorcinol (>99.5%), melamine (>99.0%), levulinic acid (>99.0%) and benzene (>99.5%) were bought from aladdin Company. Ethanol (AR) and formaldehyde (37 wt%) were procured from Sinopharm Chemical Reagent Co., LTD, (China). Active carbons were procured from Sinopharm Chemical Reagent Co., LTD (99% purity), (China) and QiXian Hui Hong Yuan Chemical Co., LTD Company (98% purity). Silica (H-18) was bought from Wacker Company. Ruthenium(III) chloride hydrate (35.0 – 42.0%) was bought from Meryer Company. Concentrated hydrochloric acid (37 wt%) was bought from QiXian Hui Hong Yuan Chemical Co., LTD Company. Unless otherwise stated, all solvents and chemicals used were of commercially available analytical grade and used without further treatment. Water used in this study was de-ionized water.

2.2. Characterization

Transmission electron microscopy (TEM) images were obtained using a JEOL-JEM-2000EX instrument. Samples for TEM observations were prepared by dispersing the sample powder in ethanol using ultrasound and then allowing a drop of the suspension to evaporate on a copper grid covered with a holey carbon film. The sample morphology was characterized by using scanning electron microscopy (SEM, JEOL JSM-7001F) with an acceleration voltage of 15 kV. EDS elemental maps were recorded on this instrument. Nitrogen-sorption measurements were performed at $-196\text{ }^{\circ}\text{C}$ on a Micromeritics ASAP 2020 analyzer. Before measurement, all samples were out gassed at $200\text{ }^{\circ}\text{C}$ under vacuum for 6 h. The specific surface area was calculated from the adsorption branch in the relative pressure range of 0.05–0.15 using the Brunauer-Emmett-Teller (BET) method. X-ray photoelectron spectroscopy (XPS) was performed under an ultrahigh vacuum on a Kratos AXIS ULTRA DLD spectrometer with Al K α radiation and a multichannel detector. C and N contents of carbon materials were determined on a Vario EL instrument. Fourier transform infrared spectroscopy (FT-IR) was recorded on a Nicolet Nexus 470 FT-IR spectrometer over the range $4000\text{--}400\text{ cm}^{-1}$ with 64 scans and a resolution of 2 cm^{-1} . Solid-state ^{13}C CP-MAS NMR spectra were recorded on an Infinityplus 300 MHz spectrometer using the following parameters: 75.4 MHz resonant frequency, 4 kHz spin rate, 4 s pulse delay, 1.0 ms contact time, and hexamethylbenzene as a reference compound. The metal content was determined by an Agilent 720ES inductively coupled plasma optical emission spectrometer (ICP-OES). Gas chromatography (GC) analysis was carried out on an Agilent 7890A analyzer (HP-5, Agilent) with a flame ionization detector. The identification of reaction products by MS spectra was performed using GC-MS (7890B-5977A, HP-5, Agilent).

2.3. Synthesis of honeycombed MPCs

1.5 mmol of resorcinol (R) was dissolved in 2 mL HCl solution (2 M), followed by adding 3 mmol of melamine (M). After 1 h of sonication and stirring for 2 h at $20\text{ }^{\circ}\text{C}$, the resulting mixture was dropped onto a bed made of H-18 with an assistance of a pump. The orifice of the pump was 0.5 mm in diameter. The produced droplets were then rolled on the bed, yielding liquid marbles. The marbles were placed in the upper layer of a 100 mL Teflon-lined autoclave, at the bottom of which contained

2 mL of 37 wt% aqueous formaldehyde (F). The autoclave was vacuumized rapidly and then was allowed to stand at 75 °C. After 10 h, the particulate materials were treated in a vacuum oven at 100 °C for a further 10 h, to remove any water. The as-synthesized MRF resin microspheres were heated up to 350 °C with temperature ramped at a rate of 2 °C min⁻¹, and then maintained at this temperature for 2 h in a nitrogen flow, and then further heated up to 600 °C with temperature increasing at a ramping rate of 1 °C min⁻¹. They were then maintained at this temperature for 3 h, allowing them to carbonize.

2.4. Structural tuning of MPCS

2.4.1. By adjusting the molar ratio of C precursor

Keeping the amount of melamine unchanged, the resorcinol was increased from 1 mmol, 1.5 mmol, 2 mmol, or 3 mmol, respectively. Namely, the molar ratios of M/R are correspondingly 3, 2, 1.5 or 1. Other procedures are the same as the synthesis of honeycombed MPCS.

2.4.2. By the time of formaldehyde vapor treatment

The polymerization time was varied from 5 min to 11 h (M/R=2 for this series of sample). Other procedures are the same as the synthesis of honeycombed MPCS.

2.5. Particle size tuning

The size of MPCS was tuned through variation of feeding rate of the syringe pump in combination with the inner diameter of the syringe. For 1 mm, flow rate was 0.5 ml min⁻¹ or the inner diameter of the syringe was 0.3mm; For 2 mm, flow rate was 0.3 ml min⁻¹ or the inner diameter of the syringe was 0.5mm; For 3 mm, flow rate was 0.1 ml min⁻¹ or the inner diameter of the syringe was 0.7mm.

2.6. Preparation of the Ru/MPCS catalyst

Typically, 20 mg RuCl₃·3H₂O was dissolved in the liquid marbles prior to vapour treatment. The subsequent procedures were the same as those above. The resultant Ru-containing MRF resin was heated to 350 °C at a ramping rate of 2 °C min⁻¹ and maintained at this temperature for 2 h in 5% H₂/95% N₂ flow. Following this step, the temperature was further increased to 600 °C at a rate of 1 °C min⁻¹. The resin was maintained at 600 °C for a further 3 h. The obtained sample is denoted as Ru/MPCS throughout the rest of the paper.

2.7. Preparation of the Ru/AC catalyst

Typically, 24 mg $\text{RuCl}_3 \cdot 3\text{H}_2\text{O}$ was dissolved in 12 mL deionized water. Then 300 mg active carbon (from Sinopharm Chemical Reagent Co., Ltd or QiXian Hui Hong Yuan Chemical Co. Ltd Company) was added into the above solution, leading to a suspension. After being stirred at room temperature for 12 h, this suspension was dried through removal of liquid under vacuum at 45 °C and maintained at this temperature for 3 h. The resultant solid was dried at 100 °C for 10 h and then heated to 200 °C at a ramping rate of 5 °C min^{-1} and maintained at this temperature for 2 h in a 5% H_2 / 95% N_2 flow.

2.8. Hydrogenation of levulinic acid (LA)

In a typical reaction, 0.9 g LA, 14.86 mg catalyst and 3 g of water were added to a 100 mL Teflon-lined steel autoclave. Before reaction, the autoclave was sealed and flushed with H_2 five times to remove any air. After being charged with a 3.5 MPa H_2 at room temperature, the autoclave was then heated to 110 °C while being stirred (1000 rpm) for reaction to occur. The autoclave was allowed to cool to room temperature after reaction. The product was collected after evaporating water. The products were analyzed by a gas chromatograph. The catalyst was isolated from the reaction mixture via filtration, thoroughly washed with water five times, and then dried at 40 °C under a vacuum, ready to be used in the next reaction cycle.

2.9. Hydrogenation of benzene to cyclohexane in a fixed-bed reactor

In a typical reaction, 0.519 g catalyst (with 0.88 wt% Ru) was packed in a fixed-bed, at bottom of which was filled with glass wool. Prior to hydrogenation of benzene to cyclohexane, the catalyst was flushed with H_2 at 3.5 MPa to remove air. Subsequently, a solution of benzene as mobile phase was pumped through the inlet of the column reactor at a given flow rate at 0.017 mL h^{-1} and was allowed to pass through the column reactor whose temperature was kept at 110 °C. The outflow from the outlet of the column reactor was sampled for GC at intervals. The product was further confirmed with GC MS.

3. Results and Discussion

3.1. MPCS preparation

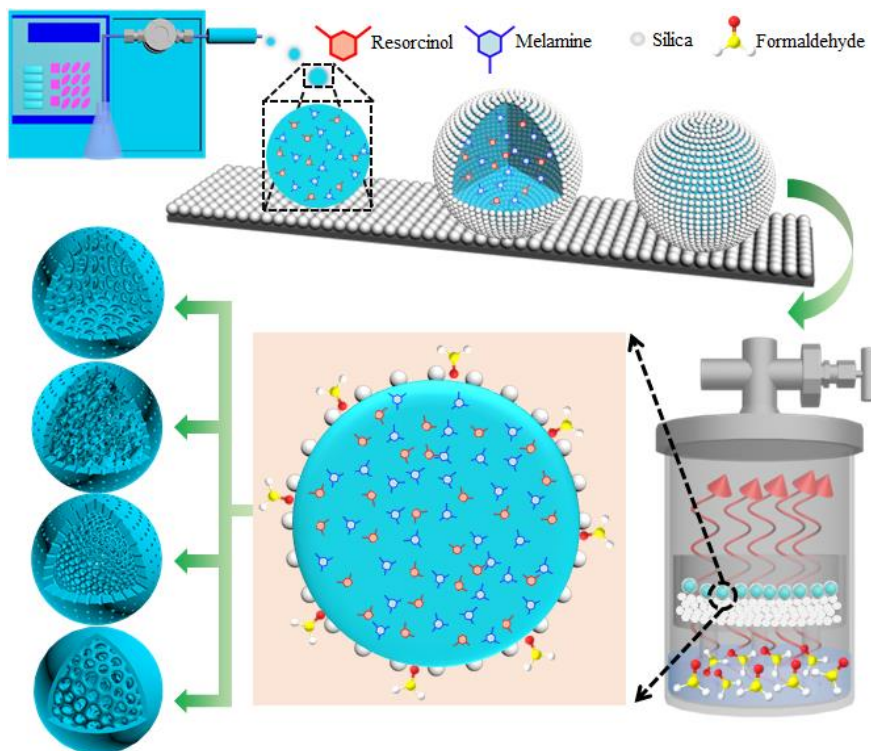


Fig. 1. Schematic illustration of the preparation of MPCS. Droplets of a hydrochloric acid solution containing resorcinol (R) and melamine (M) are dropped onto a bed made of H-18 powders with the aid of a syringe pump, followed by rolling on the bed and then treated with formaldehyde (F) vapour. Changing synthesis conditions leads to different interior structures of MPCS.

To break through the size limit of carbon microspheres reported, so far in the literature, we harness a so-called liquid marble phenomenon, which allows for compartmentalization of a liquid as much as a few to hundreds μm , in the form of droplets having hydrophobic nanoparticles adsorbed on their surfaces [34-35]. Benefiting from the presence of a hydrophobic layer on the surface, the liquid marbles have good mechanical strength against deformation in comparison to bare droplet, and as such can avoid any leakage of liquid [36-37]. Such properties are expected to facilitate any manipulation of liquid marbles without deformation, thus providing for better tuning of their interior liquid contents at will. Commercial silica particles (H-18, 16 nm in size, TEM images in Fig. S1 in the Supporting Information) were derived to hydrophobic particles for preparing liquid marbles (See Experimental Section). In the past years, doping heteroatoms (e.g., boron, phosphorous, sulfur and nitrogen) into synthetic carbon framework has been proved as an efficient strategy to improve the performance of

carbon materials [38]. As depicted in Fig. 1, the whole procedure comprises of mainly three steps: liquid marble preparation, vapour treatment and carbonization. First, droplets of a hydrochloric acid solution, containing resorcinol (R) and melamine (M) are dropped onto a bed made of H-18 powders using a syringe pump, followed by rolling on this bed. The mixture of R and M was chosen as carbon precursors because melamine-formaldehyde resins (MF) results in N functionality and high mechanical robustness [39-42]. Due to the gas / liquid interfacial adsorption, the hydrophobic H-18 particles were picked up by the droplets and adsorbed to their surfaces during the rolling. This formed a hydrophobic layer around the surface of droplets leading to formation of liquid marbles. The as-prepared liquid marbles were treated with formaldehyde (F) vapor in a designed autoclave (Fig. 1), thus generating melamine-resorcinol-formaldehyde (MRF) resin microspheres. Finally, the carbonization of the resin microspheres produced MPCs. The preparation method holds promises for large-scale fabrication of carbon microspheres because of its operational simplicity and the good level of its controllability.

3.2. Characterization.

The morphology and interior structure of the obtained MPCs were observed by scanning electron microscope (SEM) and transmission electron microscope (TEM). For example, the obtained MPCs (where the molar ratio of M to R is 2) was chosen here for a more detailed characterization. Liquid marble-derived MRF resin microspheres are yellow and discrete, being 2 mm in size. After carbonization, the resin microspheres were transformed to uniform carbon microspheres, without any apparent shrinkage in their size (Fig. 2A, B and Fig. S2). The uniform spherical morphology is attributed to the robustness and non-stick features of the liquid marbles, each of which acted as an individual microreactor during the polymerization and carbonization, therefore avoiding any fusion. The key role of liquid marble for obtaining uniform microspheres is highlighted by a comparative experiment, where bare droplets (without adsorption of H-18 nanoparticles on the surfaces) led to a collapsed, nonuniform morphology (Fig. S3). The surface of MPCs is relatively smooth, while its interior exhibits a honeycomb-like porous structure. The macropores of 5~25 μm are discerned throughout the interior of the particles, as shown by the SEM image of their cross-section (Fig. 2C-

G). Furthermore, TEM inspection reveals that there are abundant mesopores whose size is about 6 nm (Fig. 2H). N₂ sorption analysis further reveals the mesoporous and microporous porosity nature of MPCs, as evidenced by a type-IV curve of isotherms with relatively steep adsorption at low and moderate pressures (Fig. 2I). Such sorption isotherm is indicative of the presence of both micropores and mesopores. The determined BET specific surface area and pore volume are 433 m² g⁻¹ and 0.202 cm³ g⁻¹ (mesopore volume, 0.046 cm³ g⁻¹; micropore volume, 0.156 cm³ g⁻¹), respectively. The mesopore and micropore sizes were measured to be 6.3 nm (BJH method) and 0.9 nm (DFT method), respectively (Fig. 2J). For the samples pyrolyzed at 700 and 800 °C, the determined BET specific surface areas are 362 and 238 m² g⁻¹ while their mesopore and micropore sizes are measured to be 4.1, 4.1 nm (BJH method) and 0.73, 0.49 nm (DFT method), respectively. Apparently, compared with MPCs-600, S_{BET} of MPCs-700 and MPCs-800 decrease significantly. This might be induced by thermally driven shrinkage of the carbonaceous matrix and collapse of microporosity [43]. It is worth mentioning that this integration of macropores, mesopores and micropores does not need any templates or other operations, such as solvent exchange for generating macropores [44-45]. More importantly, the fabricated honeycombed MPCs is very robust, and can withstand compressive forces as high as 14.6 N per particle. To the best of our knowledge, this compressive strength places our honeycombed MPCs at the top end of the carbon microsphere so far reported in the literature [24].

The elemental mappings by TEM reveal that C and N elements are uniformly distributed throughout the particles (Fig. 3A1-A4). Such a uniform distribution is further supported by the X-ray photoelectron spectroscopy (XPS) results that the N fraction in the interior of MPCs is very close to that in the shell (Fig. 3B and Fig. S4A). Meanwhile, XPS analysis also provides the information about N-bonding microenvironments (Fig. 3C and Fig. S4B). The N1s peak could be deconvoluted into three peaks, which correspond to different chemical states of N. The peak at around 398.2 eV is attributed to pyridinic-N, which is assignable to the neutral imine nitrogen of a triazine ring; the peak at around 400.5 eV is ascribed to graphitic N, corresponding to neutral amine nitrogen atoms; the peak at around 399.0 eV is assigned to the pyrrolic-N [41]. These N bonding states imply that N was incorporated into MPCs through the chemical linkages during the polymerization or carbonization.

Moreover, Raman spectrum of MPCS displays two broad peaks which are typically found in carbonaceous materials. One is the D band around 1350 cm^{-1} and the other is the G band around 1600 cm^{-1} (Fig. 3D).

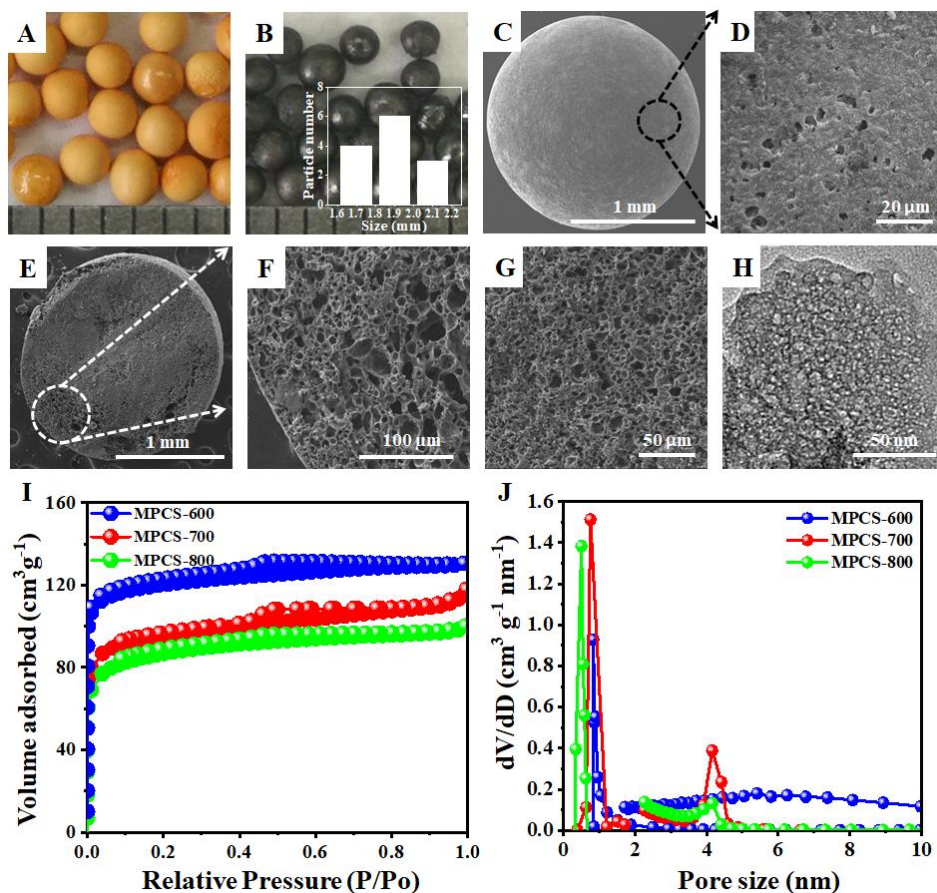


Fig. 2. Structural characterization of MRF resin microspheres and honeycombed MPCS. (A) Appearances of MRF resin microspheres. (B) Appearances of honeycombed MPCS after carbonization at $600\text{ }^{\circ}\text{C}$ (the inset is particle size distribution). (C) SEM image for a single honeycombed MPCS particle. (D) SEM image showing the surface of honeycombed MPCS. (E) SEM image showing the interior structure of honeycombed MPCS, after being cut deliberately. (F) and (G) SEM images showing the interior structure of honeycombed MPCS. (H) TEM image of honeycombed MPCS. (I) N_2 adsorption-desorption isotherms of honeycombed MPCS. (J) Pore size distribution plots of honeycombed MPCS.

The successful polymerization of M and R into the resin network is confirmed by Fourier transform infrared spectroscopy (FT-IR) results (Fig. 3E). The peak for $\text{C}=\text{C}$ stretching vibrations at 1620 cm^{-1} was observed for the above prepared MRF resin, while this peak does not appear in the MF

resin. Meanwhile, a new strong absorption band at 1560 cm^{-1} representing the aromatic C-N stretching vibrations in the triazine unit appeared, otherwise not present in RF resin. The simultaneous presence of the characteristic peaks of both MF resin and RF resin indicates the successful incorporation of the two monomers into the resin microspheres. The solid state ^{13}C NMR spectra of MRF resin further confirms that this resin consists of sp^2 carbons which are assigned to the triazine ring ($\sim 165\text{ ppm}$) or benzene ring ($\sim 150\text{ ppm}$ and $\sim 116\text{ ppm}$) (Fig. 3F). These findings provide additional support that M and R relevant units are linked via covalent bonding. The N content in MPCs was determined to be as high as 14.73 %, by elemental analysis (Fig. S4C).

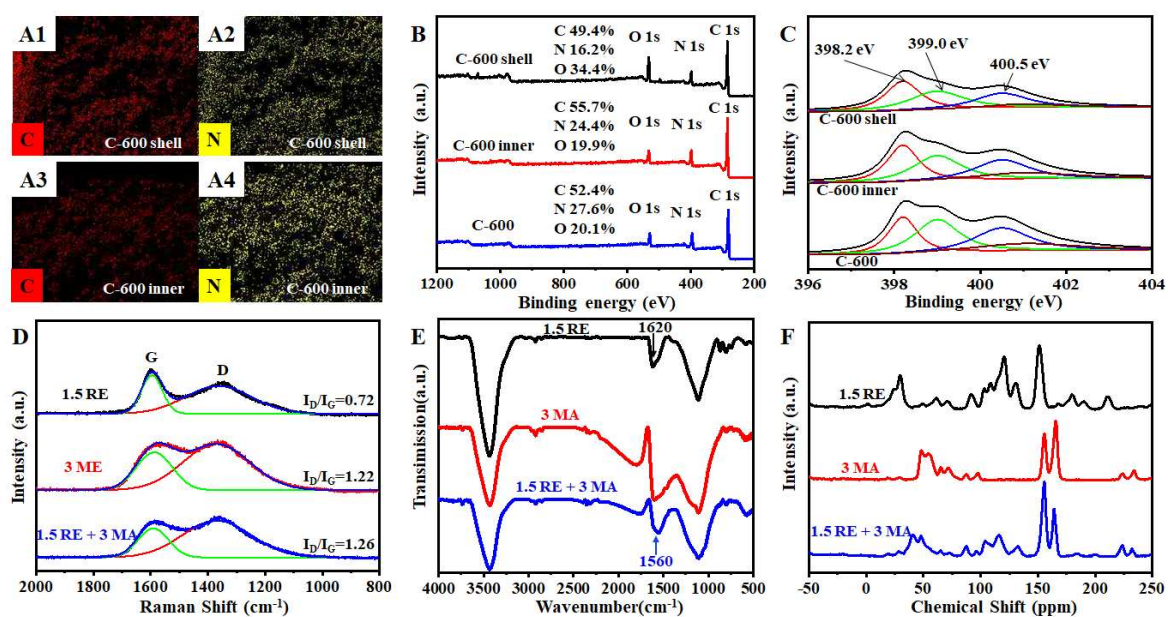


Fig. 3. Compositional characterization of honeycombed MPCs and relevant resins. (A1) C elemental mapping showing the shell of honeycombed MPCs. (A2) N elemental mapping showing the shell of honeycombed MPCs. (A3) C elemental mapping showing the interior of honeycombed MPCs. (A4) N elemental mapping showing the interior of honeycombed MPCs. (B) XPS spectra recorded at the centre, shell of honeycombed MPCs and the honeycombed MPCs milled sufficiently to obtain an average. (C) XPS N1s spectra recorded at the centre, shell of honeycombed MPCs and the honeycombed MPCs milled sufficiently to obtain an average. (D) Raman spectra of carbon materials prepared from RF resin and MF resin, and honeycombed MPCs. (E) FTIR spectra of RF resin, MF resin and MRF resin. (F) ^{13}C solid NMR spectra of RF resin, MF resin and MRF resin.

3.3. Tuning of structure by adjusting the molar ratio of C precursor

With the above interesting results, we next explore the possibility of tuning the structure of MPCS. It was found that the interior structure of MPCS strongly depended on the molar ratio of M/R. When a molar ratio of 3 was applied, foam-like MPCS was obtained and many micron-sized holes were observed in the interior of fabricated particles (Fig. 4A). The M/R ratio was then adjusted to 2, this time leading to honeycombed MPCS, as was discussed before. When the M/R was decreased further to 1.5, a big cavity appeared in the interior of the synthesized particles (Fig. 4B). In the case of the M/R=1, a hollow structure with a dense shell was formed instead (Fig. 4C). N₂ sorption analysis also gave more information regarding the changes in porosity (Fig. 4E and Fig. S5). The specific surface area and pore size were also both related to the molar ratio of M/R. For the case with the M/R ratio of 3, specific surface area and pore size are 396 m² g⁻¹ and 6.7 nm, respectively. When the molar M/R ratio was 2, the specific surface area reached a maximum value (433 m² g⁻¹) and the pore size decreased down to 6.3 nm. Further decreasing the M/R ratio to 1.5 and then to 1, caused both the specific surface area and the pore size to decline further.

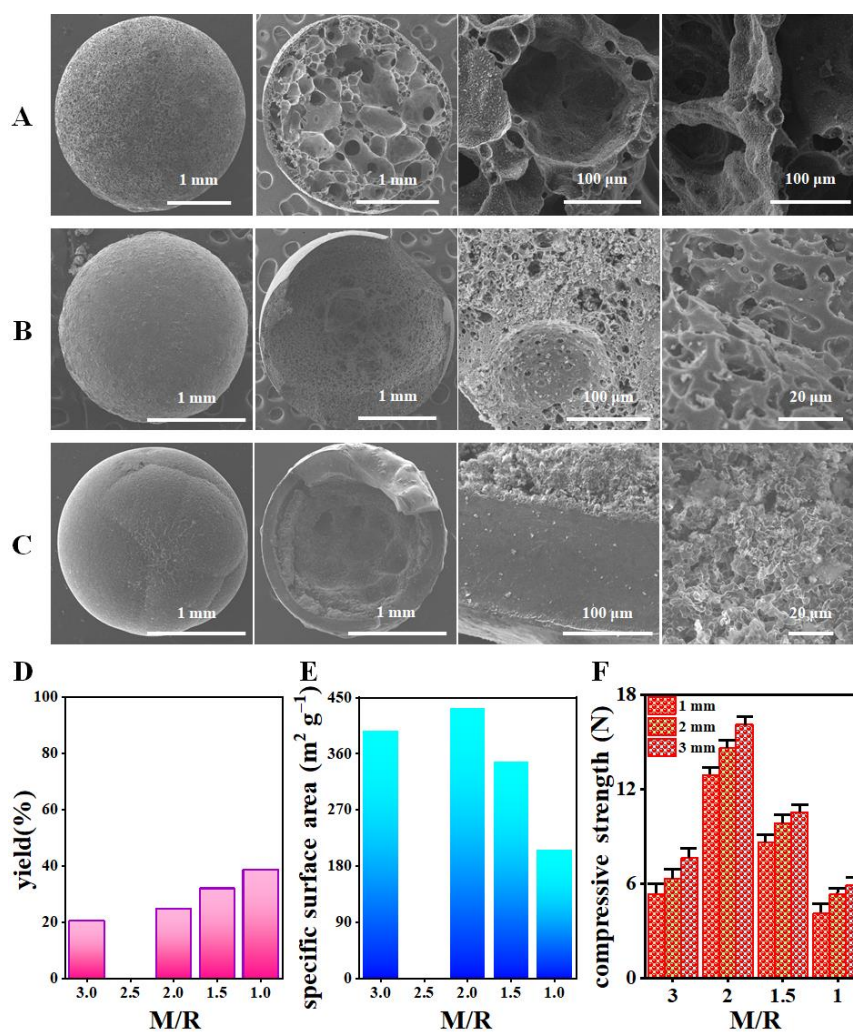


Fig. 4. Characterization of MPCS prepared with different molar ratios of M to R. (A) SEM images showing a single microsphere and its interior structure fabricated at a molar ratio of $M/R = 3$. (B) SEM images showing a single microsphere and its interior structure when the ratio of $M/R = 1.5$. (C) SEM images showing a single microsphere and its interior structure for a molar ratio of $M/R = 1$. (D) Carbonization yields of MF resin, RF resin and MRF resins at several different molar ratios. (E) Specific surface area for MPCS prepared with different molar ratios of M to R. (F) Compressive strength for MPCS prepared with different molar ratios of M to R and different size.

Interestingly, these MPCS particles exhibit different mechanical strengths. The compressive strengths for a single particle of foam-like MPCS or a cavity-containing MPCS or a hollow MPCS were determined to be 6.3, 9.8 and 5.3 N, respectively (Fig. 4F). The change in compressive strengths can be explained in terms of the interior pore structures and the molar ratio of M/R . We found that compressive strength gradually increased with the molar ratio of M/R , reaching a maximum, and then it began to go down. The increase of M content caused high rigidity [39]. This is supported by a comparative experiment (Fig. S6 and Fig. S7), where the carbon spheres fabricated via polymerization of M with F are found to be mechanically more robust than the ones made via polymerization of R with F. However, further increasing the M/R ratio resulted in the formation of a loose foam-like structure which has a lower mechanical strength. The maximum mechanical robustness is the result of a trade-off between the value of the used M/R ratio and the desired interior structure.

3.4. Tuning of structure by using the duration time of formaldehyde vapour treatment

Another interesting observation is that the interior structure of MPCS is a function of the time of formaldehyde (F) vapour treatment. After 5 min of formaldehyde vapour treatment (with $M/R=2$ applied for this series of samples), hollow MPCS with a crust of about 0.5 mm in thickness was obtained (Fig. 5A). When the treatment time was increased to 15 min, the cavity dimension gradually decreased because more polymer was formed (Fig. 5B). When the treatment time was prolonged to 7 h, the cavity became gradually filled (Fig. 5C). Further increasing the treatment time to 11 h, the distinct morphology of honeycombed MPCS was obtained (Fig. 5D). This time-dependent change in

the interior architecture can be explained by the fact that the longer time of F vapour treatment leads to more F diffusing from the droplet surface to its interior, thus becoming available for polymerization. Meanwhile, the specific surface area gradually increased with the treatment time and levelled off till the treatment time of 10 h (Fig. 5E and Fig. S8). The mechanical strength also increased at first and then begins to slightly decreased with changing the time of vapour treatment (Fig. 5F). Obviously, such a flexible method becomes possible due to the use of the liquid marble strategy in conjunction with vapour treatment.

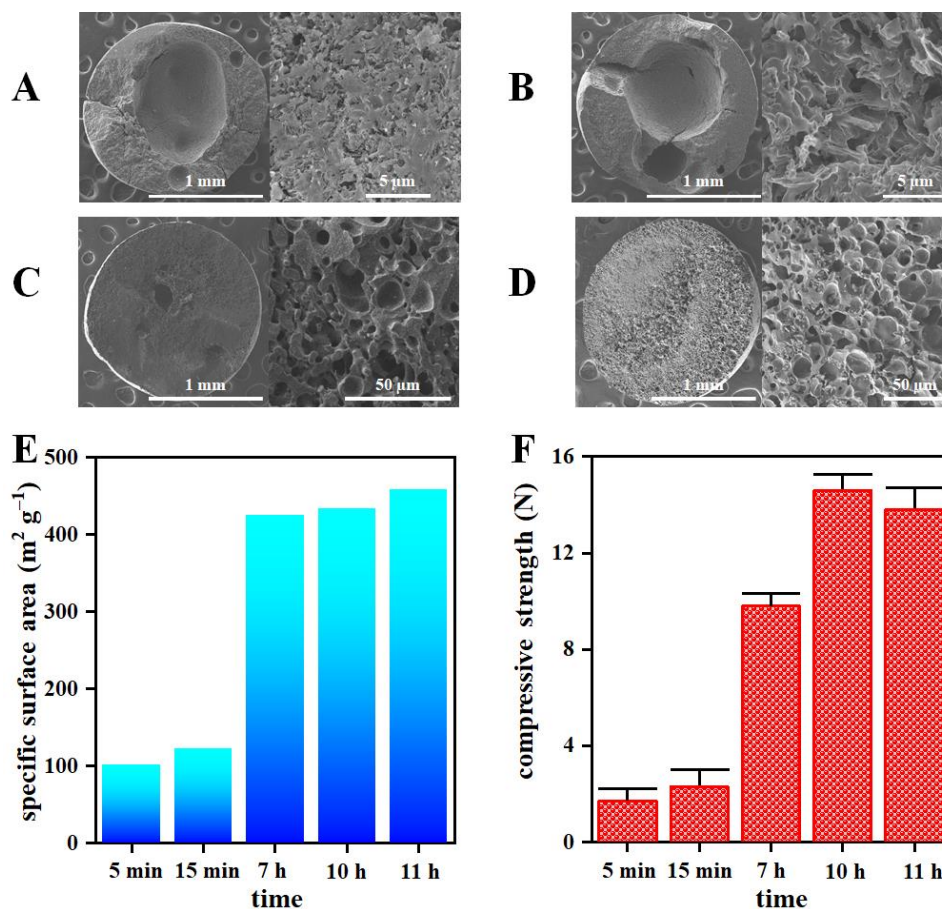


Fig. 5. Characterization of MPCs prepared with F vapour treatment for different time scales. (A) SEM images showing the interior structure of MPCs and its microregion, prepared after 5 min of vapour treatment. (B) SEM images showing the interior structure of MPCs and its microregion, fabricated with 15 min of vapour treatment. (C) SEM images showing the interior structure of MPCs and its microregion, involving 7 h of vapour treatment. (D) SEM images showing the interior structure of MPCs and its microregion, produced after 11 h of vapour treatment. (E) Specific surface area for MPCs prepared via different times of F vapour treatment. (F) Compressive strength for MPCs prepared via different times of F vapour treatment.

3.5. Particle size tuning

Besides the interior structure and N-functionalization, the size of MPCs can also be tuned through variation of the size of the liquid marble. Lower feeding rate of the syringe pump and larger inner diameter of the syringe lead to larger liquid marbles and further to large particles. The average diameter of MPCs could be regulated from 1 mm to 3 mm upon decreasing the flow rate from 0.5 to 0.1 mL min⁻¹ or increasing the inner diameter of the syringe from 0.3 mm to 0.7 mm, hence highlighting the additional flexibility of our synthesis protocol (Fig. 6). Despite the engineered changes in the particle size, the specific surface area and pore size are not altered significantly (Fig. S9). To the best of our knowledge, this is the first time that large carbon microspheres of this size have been achieved through such a flexible and easily implement procedure. The compressive strengths for a single particle of honeycomb-like MPCs from 1 mm to 2 mm to 3 mm were determined to be 12.9, 14.6 and 16.1 N, respectively (Fig. 4F). It can be seen that the compressive strength gradually increased with the increasing of particle size. Moreover, the foam-like MPCs, cavity-containing MPCs and hollow MPCs also exhibited the same strength tendency by varying their particle sizes.

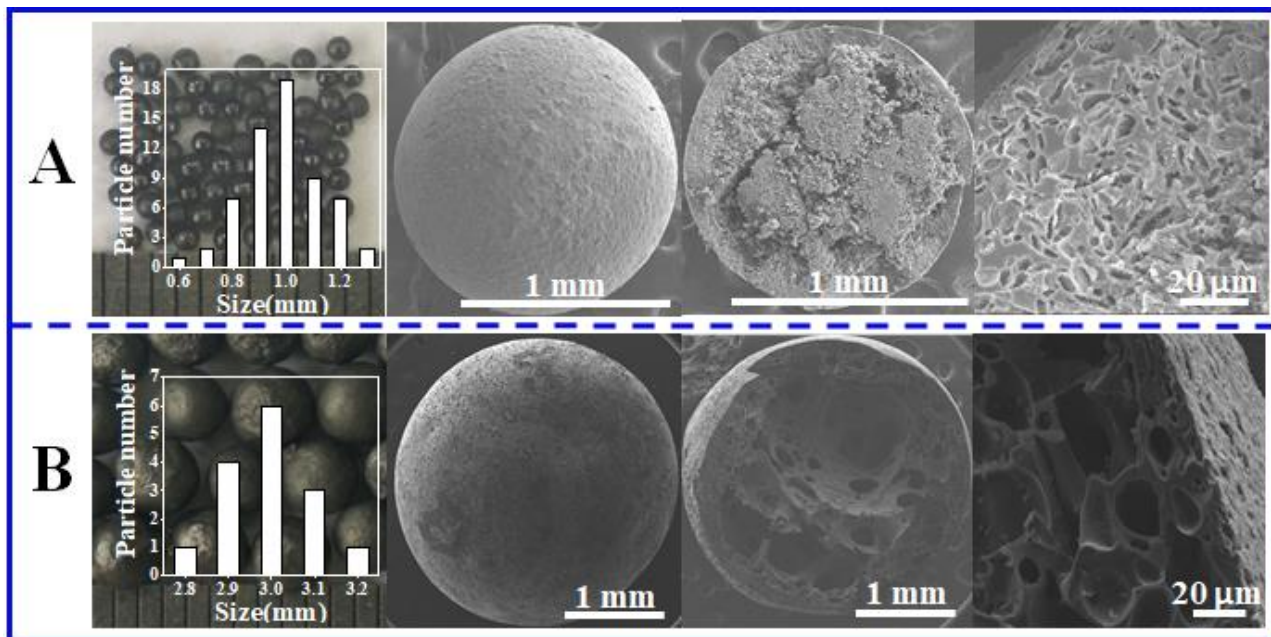


Fig. 6. Characterization of the honeycombed MPCs with different particle sizes. (A) SEM images for a single microsphere of 1 mm and its interior structure (the inset is particle size distribution). (B) SEM images for a single microsphere of 3 mm and its interior structure (the inset is particle size distribution).

3.6. Mechanism for pore and structure formation

Based on the above observations, we propose a formation mechanism for the structural evolution of MPCs. As illustrated in Fig. 7A, the polymer skeleton growth within the liquid marbles undergoes three distinct stages. First, the primary polymerization of M or R with F takes place under the assistant of acid, thus forming methylene or methylene ether bridged oligomers. These further grows to form small clusters [41]. Then, the small clusters act as nucleation sites to continue growing and crosslinking together, eventually giving rise to 3-D gel networks within the confinements of the liquid marbles. With the increasing molecular weight of polymers, microphase separation within the compartments is induced because of the gradual decrease in solubility of the cross-linked polymers in water. At the following stage involving carbonization, the micropores are created due to the release of volatiles from decomposition of resin. The mesopores and macropores are formed arising from microphase separation during polymerization and carbonization process due to the shrinkage of polymer network units, depending on the extent of compactness or degree of openness of aggregated networks. Note that the polymerization rate of R with F is much faster than that of M with F. Also, the number of nucleation sites is significantly altered when one varies the M/R ratio. The difference in their polymerization activity makes it possible to tune the polymer network by changing the molar ratio. This effect is also reflected in the results of the comparative experiments where only M or R were used as the sole polymer monomers (Fig. S6). The carbon materials synthesized solely from R or from M exhibited specific surface area of 221 or 11 $\text{m}^2 \text{g}^{-1}$, which are both much lower than those seen for a mixture of M and R. As presented in Fig. 7B, at the high M/R ratios, the formed nuclei are fewer yet large in size owing to the lower activity of M. As a result, the polymerization rate and the degree of crosslinking occurs relatively slowly, leading to more macropores and less mesopores. At the same time, the MF units are thermally more susceptible in comparison to RF units, generating more volatile compounds during carbonization (related to carbonization yield as presented in Fig. 3D and Fig. S2). Therefore, the high ratio of M/R gives rise to more abundant pores (Fig. S10). As the M/R ratio decreases, more nucleation sites become available for polymerization and the degree of cross-linking also improves. This leads to denser polymer networks. Accordingly, a final structure with

less macropores, more mesopores/micropores and high specific surface areas are achieved.

In parallel, the compartmentalisation within liquid marbles also plays a significant role in the architectural evolution. As illustrated in Fig. 7C, molecules of F in the gaseous phase diffuse towards the interfaces made by liquid and gas phases, encountering R and M molecules at these interfaces where the polymerization occurs. The process forms a shell around the liquid marbles. As the polymerization proceeds further, the consumption of M and R means that their concentration drops to lower values at the surface than within the droplet interior. Nevertheless, water evaporation drives the M, R and polymer clusters to be continuously transported from interior towards the surface of the droplet. This technique for the initial polymerization occurring first at the interface and then subsequently in the interior provides an opportunity to tune the interior structures within MPCs by simply changing the time for F vapor treatment. Also, at the high M/R ratios, the polymerization takes place relatively slow, where F molecules have sufficient time to diffuse more deeply into the interior, hence leading to a relatively more uniformity throughout the particles. In contrast, at the low M/R ratios, the polymerization proceeds faster and F molecules have no sufficient time to diffuse into the interior prior to being utilized close to the surface. This results in the formation of hollow structures. Note that the continuous escape of water vapour from the interior liquid marbles also makes the interconnection of the formed pores possible.

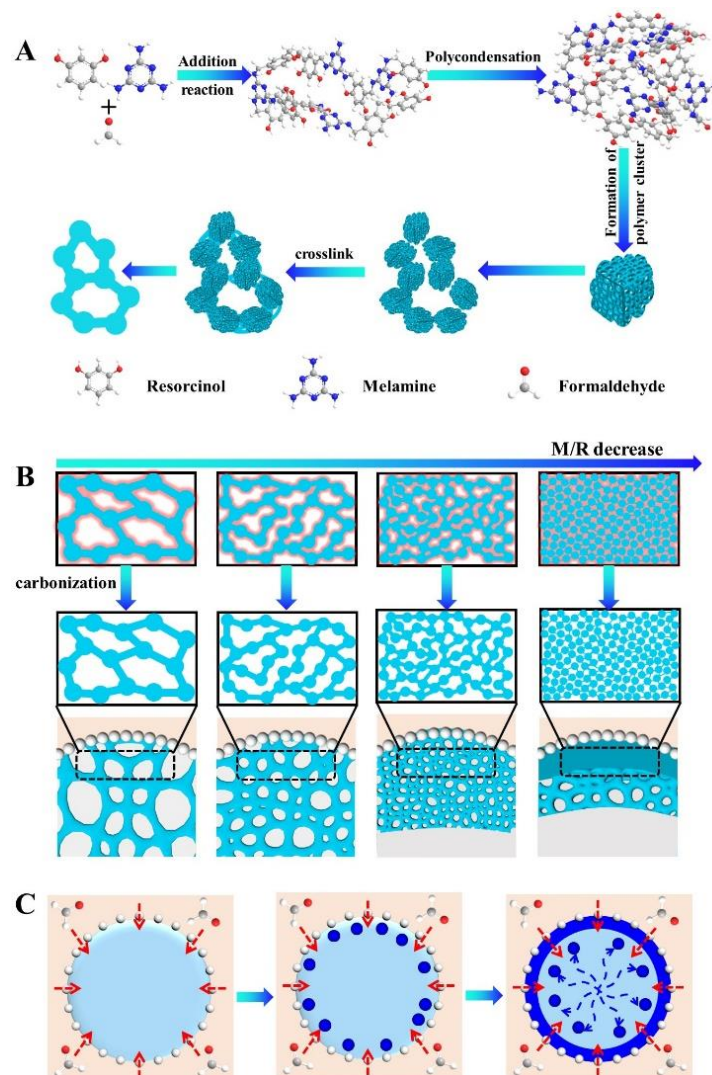


Fig. 7. Schematic illustration of the formation mechanism of MPCS. (A) Formation of polymer cluster and crosslinking of such clusters. (B) Evolution of the interior pores of MPCS particles, both before and after carbonization with different molar ratios of M to R leading to the changes in the structure of the polymer network. (C) Water evaporation within the compartment of liquid marbles affecting structural evolution.

3.7. Catalytic applications of honeycombed MPCS

To evaluate the ability of our method to fabricate suitable carbon-based catalysts, we first chose as an example Ru-catalyzed hydrogenation of levulinic acid (LA) to γ -valerolactone (GVL), which is a key reaction for biomass utilization (Fig. 8A). Despite extensive investigation, the most of the available existing catalysts for this reaction still suffer from deactivation and Ru leaching.

Our liquid marble method allowed Ru to be in situ embedded into the honeycombed MPCS. This was achieved by adding $\text{RuCl}_3 \cdot 3\text{H}_2\text{O}$ into the aqueous solution prior to the preparation of the liquid

marble, hence leading to a Ru/MPCS catalyst with homogeneous distribution of Ru throughout the body of MPCS. As the TEM image revealed (Fig. 8B), Ru nanoparticles (NPs) with an average size of 11 nm were indeed dispersed throughout the interior of MPCS. Inductively coupled plasma (ICP) analysis demonstrated that the Ru loading is 0.88 wt%. As shown in Fig. S11, the strong peaks at 484.6 and 462.3 eV are respectively ascribed to Ru0 3p_{1/2} and 3p_{3/2}, demonstrating that most of Ru have been reduced. Interestingly, the Ru 3p_{3/2} binding energy for the fresh catalyst was shifted by -0.5 eV from 462.8 when compared to the normal Ru 3p_{2/3} [47]. Such a shift may be induced by the interaction of Ru particles with N-functionalized carbon microspheres. The specific surface area of Ru/MPCS was measured to be 422 m² g⁻¹, indicating that the introduction of Ru did not affect the surface area (Fig. S12).

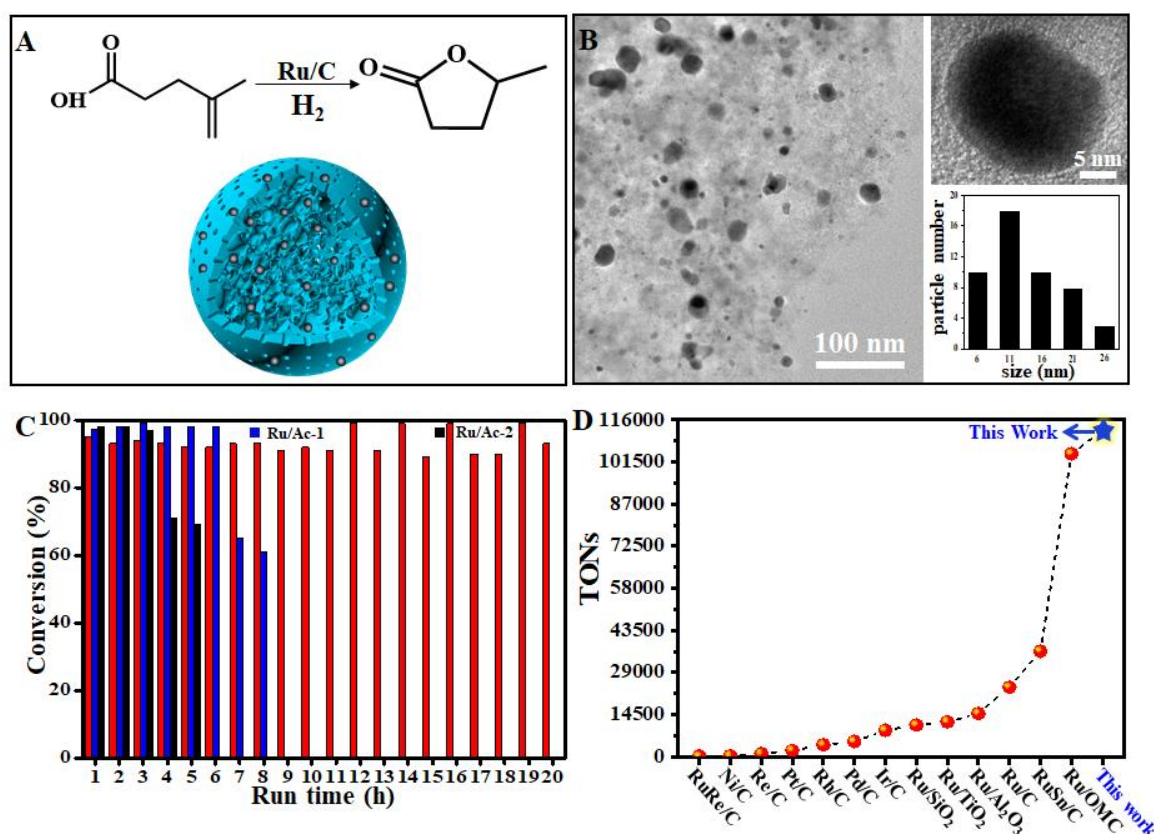


Fig. 8. Results of the LA hydrogenation achieved by the Ru/MPCS catalyst. (A) LA hydrogenation reaction and structural illustration of Ru/MPCS. (B) TEM images of Ru/MPCS and Ru nanoparticle size distribution. (C) Recyclability of our Ru/MPCS catalyst compared to two other Ru/AC catalysts (Ru/Ac-1 with Ru nanoparticles supported on the active carbon from Sinopharm Chemical Reagent Co., Ltd, Ru/Ac-2 with Ru nanoparticles supported on the active carbon from QiXian Hui Hong Yuan

Chemical Co. Ltd Company). Reaction conditions: 14.86 mg catalyst, 0.9g LA, 3 mL H₂O, 110 °C, 3.5 MPa H₂, 1000 rpm; from the first to 11th reaction, 3 h; from the 12th-13th reaction, 4 h; from the 14th-15th reaction, 5 h; from the 16th-18th, 6 h; and from the 19th-20th, 7 h. (D) Comparison of TONs of our Ru/MPCS catalyst with those for various catalyst reported in the literature [48].

LA hydrogenation was conducted at 110 °C and 3.5 MPa H₂ pressure, using S/C= 6000 (the molar ratio of LA to Ru). The Ru/MPCS gave a full conversion of LA within 3 h (Fig. 8C). This activity is better or comparable in comparison to those of most reported Ru-based carbonaceous catalysts [48]. As aforementioned (see XPS analysis), the rich electron of Ru caused by electron transfer from MPCs accounts for the high activity, which is consistent with the reported work [49-51].

Another attractive feature of this catalyst is its excellent recyclability. At the end of reaction, the Ru/MPCS catalyst can be separated from the reaction system through simple filtration although the catalyst was partially broken (Fig. S13). From the second reaction cycle to the eleventh one, the Ru/MPCS catalyst gave above 92% LA conversions. From the twelfth to the twentieth cycle, conversions of 91-99% were still possible through prolonging the reaction time to 4-7 h. After 20 cycles, the Ru loading on the Ru/MPCS was determined to be 0.77 wt% using ICP analysis (Table S1), where 87.5% Ru relative to the initial content was maintained. TEM inspection of the Ru/MPCS after 20 cycles reveals that aggregation of Ru NPs had occurred. It was found that on average the Ru NPs had grown to 16 nm in size (Fig. S14). The metal aggregation is mainly responsible for the decreased activity during consecutive recycles. For comparison, we loaded Ru NPs on commercial active carbons from Sinopharm Chemical Reagent Co., LTD (Ru/Ac-1, Fig. S15) and QiXian Hui Hong Yuan Chemical Co., LTD Company (Ru/Ac-2, Fig. S16), leading to two additional Ru/AC catalysts for us to test. In the LA hydrogenation, the former comparative catalyst lost its initial activity, and only 62 % conversion was obtained upon the 8th reaction cycles (Fig. 8C). The latter catalyst lost its initial activity even more rapidly, only providing 69 % conversion after just five reaction cycles. A contrast with our own Ru catalysts reported here, displaying a comparison of turn over numbers (TONs), have been listed in Fig. 8D. The TONs of our Ru/MPCS reached 113000, far exceeding TONs of most reported catalysts, being even slightly higher than Ru/OMC (OMC is ordered mesoporous carbon)

[48]. The outstanding stability of the Ru/MPCS catalyst may be ascribed to the Ru NPs being firmly attached to the N-functionalized carbonaceous framework during the high temperature carbonization.

Furthermore, we directly packed the Ru/MPCS catalyst in a fixed bed reactor for continuous catalysis. Industrially relevant hydrogenation of benzene to cyclohexane was examined. Our preliminary optimization of the experiment reveals that the calcination temperature significantly impacts the catalytic activity (Table S2 and Table S3). The conversion is the best at 600 °C of carbonization, and further raising carbonization temperature led to a declination in activity. This Ru/MPCS catalyst worked well in the fixed bed reactor (Fig. S17). 96% conversion of benzene and >99% selectivity to cyclohexane were maintained over a course of 480 h, where TONs reached values as high as 116000. Again this is higher than the reported catalysts in the literature [52-53]. The excellent stability may also be attributed to the N-functionalization and the in situ introduction of Ru. This allows for firmly anchoring of Ru into MPCS. The results highlight the possibility of the direct practical application of our catalyst.

4. Conclusion

We have successfully developed a simple yet effective method to fabricate millimeter-sized porous carbon microspheres (MPCS), based on the liquid marble phenomenon. Our method enables the interior architecture, pore size, N-functionality, particle size and mechanical strength to be tuned through alternation of synthesis conditions. Various interior structures including honeycomb, foam-like, cavity-containing and hollow carbon microspheres were obtained using the same fabrication process for the first time. Crucially, the mechanical strength of MPCS can reach as high as 14.6 N per particle, which makes it particularly suitable for practical applications. The key to this success is the combination of liquid marbles acting as individual microreactors, where F vapour treatment makes the polymerization process able to control. This is not achievable with virtually all the existing known methods. Furthermore, the presented method allows metals to be incorporated into the body of MPCS. The LA hydrogenation with TONs of 113000 and benzene hydrogenation with TONs of 116000 were obtained here, exemplifying the high activity and stability of the catalyst, thus highlighting the potential for practical applications. Our liquid marble method and the newly revealed insights provide

tremendous opportunity to rationally design and fabricate large-sized carbon materials and use these for realizing industrially relevant catalysts.

Acknowledgements

This work was supported by the National Natural Science Foundation of China (21925203 and 21703128).

Appendix A. Supplementary data

Supplementary data to this article can be found online at <https://doi.org/>.

Competing financial interests

The authors declare no competing financial interests.

References

- [1] D. S. Su, G. D. Wen, S. C. Wu, F. Peng, R. Schlögl, Carbocatalysis in liquid phase reactions, *Angew. Chem., Int. Ed.* 56 (4) (2017) 936-964.
- [2] T. T. Wang, Q. D. Zhao, Y. Y. Fu, C. J. Lei, B. Yang, Z. J. Li, et al., Carbon-Rich Nonprecious Metal Single Atom Electrocatalysts for CO₂ Reduction and Hydrogen Evolution, *Small Methods* 3 (10) (2019) 1900210.
- [3] J. Liu, N. P. Wickramaratne, S. Z. Qiao, M. Jaroniec, Molecular-based design and emerging applications of nanoporous carbon spheres, *Nat. Mater.* 14 (8) (2015) 763-774.
- [4] J. F. Liang, X. M. Zhang, L. Y. Jing, H. Q. Yang, N-doped ordered mesoporous carbon as a multifunctional support of ultrafine Pt nanoparticles for hydrogenation of nitroarenes, *Chin. J. Catal.* 38 (7) (2017) 1252-1260.
- [5] M. Chen, C. Yu, S. H. Liu, X. M. Fan, C. T. Zhao, X. Zhang, et al., Micro-sized porous carbon spheres with ultra-high rate capability for lithium storage, *Nanoscale* 7 (5) (2015) 1791-1795.
- [6] A. Shrestha, M. Batmunkh, C. J. Shearer, Y. T. Yin, G. G. Andersson, J. G. Shapter, et al., Nitrogen-Doped CN_x/CNTs Heteroelectrocatalysts for Highly Efficient Dye-Sensitized Solar Cells, *Adv. Energy Mater.* 7 (8) (2017) 1602276.
- [7] Y. Liu, C. Wang, J. P. Veder, M. Saunders, M. Tade, S. B. Wang, et al., Hierarchically porous cobalt-carbon nanosphere-in-microsphere composites with tunable properties for catalytic pollutant degradation and electrochemical energy storage, *J. Colloid Interface Sci.* 530 (2018) 556-566.
- [8] R. Q. Guan, L. Y. Jing, X. M. Zhang, S. Chen, N. Xue, Q. H. Yang, Microspherical nitrogen-doped carbon nanotube assembly derived from Pickering droplets, *Carbon* 148 (2019) 124-133.
- [9] L. Zhang, X. X. Liu, Y. H. Dou, B. W. Zhang, H. L. Yang, S. X. Dou, et al., Mass Production and Pore Size Control of Holey Carbon Microcages, *Angew. Chem. Int. Ed.*, 56 (44) (2017) 13790-13794.
- [10] N. N. Wu, W. J. Du, Q. Hu, S. Vupputuri, Q. L. Jiang, Recent Development in Fabrication of Co

- Nanostructures and Their Carbon Nanocomposites for Electromagnetic Wave Absorption, *Eng. Sci.*, 13 (11) (2021) 11-23.
- [11] H. S. Ju, Y. J. Hong, J. S. Cho, Y. C. Kang, Strategy for yolk-shell structured metal oxide-carbon composite powders and their electrochemical properties for lithium-ion batteries, *Carbon* 100 (2016) 137-144.
- [12] R. Liu, S. M. Mahurin, C. Li, R. R. Unocic, J. C. Idrobo, H. J. Gao, et al., Dopamine as a Carbon Source: The Controlled Synthesis of Hollow Carbon Spheres and Yolk-Structured Carbon Nanocomposites, *Angew. Chem., Int. Ed.* 50 (30) (2011) 6799-6802.
- [13] Q. Sun, B. He, X. Q. Zhang, A. H. Lu, Engineering of Hollow Core-Shell Interlinked Carbon Spheres for Highly Stable Lithium-Sulfur Batteries, *ACS Nano* 9 (8) (2015) 8504-8513.
- [14] J. Gong, J. Liu, X. C. Chen, Z. W. Jiang, X. Wen, E. Mijowska, et al., One-pot synthesis of core/shell Co@C spheres by catalytic carbonization of mixed plastics and their application in the photo-degradation of Congo red, *J. Mater. Chem. A* 2 (20) (2014) 7461-7470.
- [15] Y. H. Han, Y. G. Wang, W. X. Chen, R. R. Xu, L. R. Zheng, J. Zhang, et al., Hollow N-Doped Carbon Spheres with Isolated Cobalt Single Atomic Sites: Superior Electrocatalysts for Oxygen Reduction. *J. Am. Chem. Soc.* 139 (48) (2017) 17269-17272.
- [16] H. W. Zhang, O. Noonan, X. D. Huang, Y. N. Yang, C. Xu, L. Zhou, et al., Surfactant-Free Assembly of Mesoporous Carbon Hollow Spheres with Large Tunable Pore Sizes, *ACS Nano* 10 (4) (2016) 4579-4586.
- [17] C. H. Chen, X. F. Li, J. Deng, Z. Wang, Y. Wang, Shape Engineering of Biomass-Derived Nanoparticles from Hollow Spheres to Bowls through Solvent-Induced Buckling, *ChemSusChem* 11 (15) (2018) 2540-2546.
- [18] K. W. Tan, B. Jung, J. G. Werner, E. R. Rhoades, M. O. Thompson, U. Wiesner, Transient laser heating induced hierarchical porous structures from block copolymer-directed self-assembly, *Science* 349 (6243) (2015) 54-58.
- [19] M. H. Sun, S. Z. Huang, L. H. Chen, Y. Li, X. Y. Yang, Z. Y. Yuan, et al., Applications of hierarchically structured porous materials from energy storage and conversion, catalysis, photocatalysis, adsorption, separation, and sensing to biomedicine, *Chem. Soc. Rev.* 45 (12) (2016) 3479-3563.
- [20] K. Min, W. Choi, C. Kim, M. Choi, Oxidation-stable amine-containing adsorbents for carbon dioxide capture, *Nat. Commun.* 9 (2018) 726.
- [21] W. Choi, K. Min, C. Kim, Y. S. Ko, J. W. Jeon, H. Seo, et al., Epoxide-functionalization of polyethyleneimine for synthesis of stable carbon dioxide adsorbent in temperature swing adsorption, *Nat. Commun.* 7 (2016) 12640.
- [22] K. Min, W. Choi, M. Choi, Macroporous silica with thick framework for steam-stable and high-performance poly(ethyleneimine)/silica CO₂ adsorbent, *ChemSusChem* 10 (11) (2017) 2518-2526.

- [23] M. Li, Y. N. Zhang, X. L. Wang, W. Ahn, G. P. Jiang, K. Feng, G. Lui, Z. W. Chen, Gas Pickering Emulsion Templated Hollow Carbon for High Rate Performance Lithium Sulfur Batteries, *Adv. Funct. Mater.* 26 (46) (2016) 8408-8417.
- [24] Y. P. Chong, K. Liu, Y. Liu, J. T. Wang, W. M. Qiao, L. C. Ling, et al., Highly Efficient Removal of Bulky Tannic Acid by Millimeter-Sized Nitrogen-Doped Mesoporous Carbon Beads, *AIChE J.* 63 (7) (2017) 3016-3025.
- [25] W. Xia, L. Wang, Microfluid-induced vibration and stability of structures modeled as microscale pipes conveying fluid based on non-classical Timoshenko beam theory, *Microfluid Nanofluid* 9 (4-5) (2010) 955-962.
- [26] Z. H. Jin, X. Jiang, Z. D. Dai, L. L. Xie, W. Wang, L. Shen, Continuous Synthesis of Nanodroplet-Templated, N-Doped Microporous Carbon Spheres in Microfluidic System for CO₂ Capture, *ACS Appl. Mater. Interfaces* 12 (47) (2020) 52571-52580.
- [27] H. X. Xu, J. R. Guo, K. S. Suslick, Porous Carbon Spheres from Energetic Carbon Precursors using Ultrasonic Spray Pyrolysis, *Adv. Mater.* 24 (45) (2012) 6028-6033.
- [28] D. H. Long, F. Lu, R. Zhang, W. M. Qiao, L. Zhan, X. Y. Liang, et al., Suspension assisted synthesis of triblock copolymer-templated ordered mesoporous carbon spheres with controlled particle size, *Chem. Commun.* 23 (2008) 2647-2649.
- [29] D. W. Liu, N. Xue, L. J. Wei, Y. Zhang, Z. F. Qin, X. K. Li, et al., Surfactant Assembly within Pickering Emulsion Droplets for Fabrication of Interior-Structured Mesoporous Carbon Microspheres, *Angew. Chem., Int. Ed.* 57 (34) (2018) 10899-10904.
- [30] L. M. Guo, J. M. Zhang, Q. J. He, L. X. Zhang, J. J. Zhao, Z. Y. Zhu, et al., Preparation of millimetre-sized mesoporous carbon spheres as an effective bilirubin adsorbent and their blood compatibility, *Chem. Commun.* 46 (38) (2010) 7127-7129.
- [31] Y. Liu, M. H. Ju, C. Q. Wang, L. X. Zhang, X. Q. Liu, Preparation of monodisperse mesoporous carbon microspheres from poly-(furfuryl alcohol)-silica composite microspheres produced in a microfluidic device, *J. Mater. Chem.* 21 (38) (2011) 15049-15056.
- [32] Z. X. Wu, W. D. Wu, W. J. Liu, C. Selomulya, X. D. Chen, D. Y. Zhao, A General "Surface-Locking" Approach toward Fast Assembly and Processing of Large-Sized, Ordered, Mesoporous Carbon Microspheres, *Angew. Chem., Int. Ed.* 52 (51) (2013) 13764-13768.
- [33] X. Li, J. G. Zhou, J. T. Wang, W. M. Qiao, L. C. Ling, D. H. Long, Large-scale synthesis of mesoporous carbon microspheres with controllable structure and nitrogen doping using a spray drying method, *RSC Adv.* 4 (107) (2014) 62662-62665.
- [34] Y. F. Sheng, G. Q. Sun, J. Wu, G. H. Ma, T. Ngai, Silica-Based Liquid Marbles as Microreactors for the Silver Mirror Reaction, *Angew. Chem., Int. Ed.* 54 (24) (2015) 7012-7017.
- [35] G. McHale, M. I. Newton, Liquid marbles: principles and applications, *Soft Matter* 7 (12) (2011) 5473-5481.

- [36] X. Rong, R. Ettelaie, S. V. Lishchuk, H. G. Cheng, N. Zhao, F. K. Xiao, et al., Liquid marble-derived solid-liquid hybrid superparticles for CO₂ capture, *Nat. Commun.* 10 (2019) 1854.
- [37] X. J. Luo, X. Zhang, Y. J. Feng, Liquid Marbles: Fabrication, Physical Properties, and Applications, *Acta Phys. -Chim. Sin.* 36 (10) (2020) 1910007.
- [38] M. X. Hu, Q. Lv, R. T. Lv, Controllable Synthesis of Nitrogen-Doped Graphene Oxide by Tablet-Sintering for Efficient Lithium/Sodium-Ion Storage, *ES Energy & Environment* 3 (2019) 45-54.
- [39] H. H. Zhou, S. Xu, H. P. Su, M. Wang, W. M. Qiao, L. C. Ling, et al., Facile preparation and ultra-microporous structure of melamine-resorcinol-formaldehyde polymeric microspheres, *Chem. Commun.* 49 (36) (2013) 3763-3765.
- [40] J. T. Wang, S. Xu, Y. F. Wang, R. Cai, C. X. Lv, W. M. Qiao, et al., Controllable synthesis of hierarchical mesoporous/ microporous nitrogen-rich polymer networks for CO₂ and Cr (VI) ion adsorption, *RSC Adv.* 4 (31) (2014) 16224-16232.
- [41] X. C. Liu, S. M. Li, J. Mei, W. M. Lau, R. Mi, Y. C. Li, et al., From melamine-resorcinol-formaldehyde to nitrogen-doped carbon xerogels with micro- and meso-pores for lithium batteries, *J. Mater. Chem. A.* 2 (35) (2014) 14429-14438.
- [42] T. W. Lv, H. Y. Yan, J. K. Cao, S. R. Liang, Hydrophilic Molecularly Imprinted Resorcinol-Formaldehyde-Melamine Resin Prepared in Water with Excellent Molecular Recognition in Aqueous Matrices, *Anal. Chem.* 87 (21) (2015) 11084-11091.
- [43] M. X. Hu, Q. Lv, R. T. Lv, Controllable Synthesis of Nitrogen-Doped Graphene Oxide by Tablet-Sintering for Efficient Lithium/Sodium-Ion Storage, *ES Energy & Environ.*, 3 (53) (2019) 45-54.
- [44] B. J. Zhu, K. X., Li, J. J. Liu, H. Liu, C. G. Sun, C. E. Snape. Z. X. Guo, Nitrogen-enriched and hierarchically porous carbon macro-spheres-ideal for large-scale CO₂ capture, *J. Mater. Chem. A* 2 (15) (2014) 5481-5489.
- [45] J. Lee, J. Y. Chang, Pickering Emulsion Stabilized by Microporous Organic Polymer Particles for the Fabrication of a Hierarchically Porous Monolith, *Langmuir* 34 (39) (2018) 11843-11849.
- [46] C. Ma, X. Y. Chen, D. H. Long, J. T. Wang, W. M. Qiao, L. C. Ling, High-surface-area and high-nitrogen-content carbon microspheres prepared by a pre-oxidation and mild KOH activation for superior supercapacitor, *Carbon* 118 (2017) 699-708.
- [47] H. G. Manyar, D. Weber, H. Daly, J. M. Thompson, D. W. Rooney, L. F. Gladden, et al., Deactivation and regeneration of ruthenium on silica in the liquid-phase hydrogenation of butan-2-one, *J. Catal.* 265 (1) (2009) 80-88.
- [48] Y. Yang, C. J. Sun, Y. Ren, S. J. Hao, D. Q. Jiang, New route toward building active ruthenium nanoparticles on ordered mesoporous carbons with extremely high stability, *Sci. Rep.* 4 (2014) 4540.
- [49] Z. Meng, Y. Liu, G. X. Yang, Y. H. Cao, H. J. Wang, F. Peng, et al., Electron-Rich Ruthenium on Nitrogen-Doped Carbons Promoting Levulinic Acid Hydrogenation to γ -Valerolactone: Effect of Metal-Support Interaction, *ACS Sustainable Chem. Eng.* 7 (19) (2019) 16501-16510.

- [50] S. Armenise, L. Roldán, Y. Marco, A. Monzón, E. García-Bordejé, Elucidation of Catalyst Support Effect for NH₃ Decomposition Using Ru Nanoparticles on Nitrogen-Functionalized Carbon Nanofiber Monoliths, *J. Phys. Chem. C* 116 (50) (2012) 26385-26395.
- [51] C. X. Xiao, T. W. Goh, Z. Y. Qi, S. Goes, K. Brashler, C. Perez, W. Y. Huang, Conversion of Levulinic Acid to γ -Valerolactone over Few-Layer Graphene-Supported Ruthenium Catalysts, *ACS Catal.* 6 (2) (2016) 593-599.
- [52] A. Glotov, A. Vutolkina, A. Pimerzin, V. Nedolivko, G. Zasyalov, V. Stytsenko, E. Karakhanov, V. Vinokurov. Ruthenium Catalysts Templated on Mesoporous MCM-41 Type Silica and Natural Clay Nanotubes for Hydrogenation of Benzene to Cyclohexane, *Catalysts* 10 (5) (2020) 537.
- [53] H. L. Liu, R. Q. Fang, Z. Li, Y. W. Li, Solventless hydrogenation of benzene to cyclohexane over a heterogeneous Ru–Pt bimetallic catalyst, *Chem. Eng. Sci.* 122 (27) (2015) 350-359.